Available online at www.sciencedirect.com
ScienceDirect
Trans. Nonferrous Met. Soc. China 33(2023) 3871−3884
Transactions of Nonferrous Metals Society of China
www.tnmsc.cn

# Molecular dynamics simulation and experiment study on technology and mechanism of removing oil and water from aluminum chips

Jian-wen WANG[1], Shen-gen ZHANG[1], Bo LIU[1,2], Han-lin SHEN[1], Ning CHEN[3], Bo-yu WU[1], Jun LIU[1,4], Zhao-hui YAN[5]

1. Institute for Advanced Materials and Technology, University of Science and Technology Beijing, Beijing 100083, China;
2. Xinjiang Research Institute for Nonferrous Metals, Urumqi 830009, China;
3. School of Materials Science and Engineering, University of Science and Technology Beijing, Beijing 100083, China;
4. Delta Aluminium Industry Co., Ltd., Zhaoqing 526200, China;
5. Shandong Nanshan Aluminum Co., Ltd., Longkou 265713, China

Received 18 February 2023; accepted 19 July 2023

**Abstract:** The processes and mechanism of removing oil and water from aluminum chips were clarified through thermogravimetric analysis (TGA), scanning electron microscopy (SEM), response surface method (RSM) and molecular dynamics (MD). The results indicate that the cutting fluid loses mass obviously at 200−300 °C and is carbonized above 400 °C. A layered arrangement of water−surfactant−oil is formed. There are strong hydrogen bonds, strong and weak van der Waals (vdW) forces between O—H in surfactant and O atom in water at 1.63, 3.27 and 5.05 Å, respectively. With the increase of temperature, the weak interaction vdW force is vanished, and the hydrogen bond is reduced. The strong vdW force and hydrogen bonds are broken and the layered arrangement of water−surfactant−oil interface is unstable and destroyed above 277 °C. The removal rate of water and oil is up to 99.7% when the chips are heated at 370 °C for 70 min with 3 cm loading thickness.

**Key words:** water removal; oil removal; machining chips; molecular interface; recycled aluminum alloy; mechanism

## 1 Introduction

Aluminum alloys are the second widely used alloys in the world. There are 3−5 wt.% of the casting chips generated during the machining process [1]. These chips are important secondary resources. They can be recycled by hot extrusion in solid state [2−6] or remelted [7] with addition of elements, scraps and/or primary alloy [8]. But the chips contain water and oil due to the use of cutting fluid in the machining process [9]. The water and oil seriously affect the properties of the recycled products, resulting in a reduction in the grade of recycled aluminum as casting products [10]. Removing water and oil is a key pretreatment of the recycling of aluminum chips.

Current methods of removing water and oil are centrifugation, washing, extraction, ultrasonication, baking, distillation and so on. Chemical reagents are used to demulsify and separate oil and water in the washing method. Organic solvents are used to separate different oils in the extraction method [11]. The fine micro bubbles [12] created by ultrasonic waves are used to remove oil and water on the solid surface in the ultrasonication. Water and oil are

**Corresponding author:** Shen-gen ZHANG, Tel: +86-10-62333375, E-mail: zhangshengen@mater.ustb.edu.cn; Bo LIU, Tel: +86-10-82376835, E-mail: liubo@ustb.edu.cn
DOI: 10.1016/S1003-6326(23)66377-0

evaporated in the baking method. The above methods are usually used in combination in practical applications. For example, KHAMIS et al [13] and PANDEY et al [14] used acetone solution to clean aluminum chips in ultrasonic bath. HYODO et al [15] washed 7050 chips with alkaline cleaner and carefully dried with propane flame. KORE et al [16] crushed 6082 aluminum chips and sieved them into particles smaller than 5 mm. The particles were washed with soap and acetone in ultrasonic bath. However, methods used in the above studies are complicated and time-consuming. In addition, the detergent and oil will produce new wastes, such as wastewater [17]. The baking method has high efficiency and low cost. But the health of machine operators can be impaired when they breathe in or swallow oil mist [18], even in the stage of low temperature baking.

Distillation has high efficiency and no secondary pollution compared with methods above. However, the parameters for aluminum machining chips are still unclear. Molecular dynamics (MD) provides a detailed insight into the oil−water interface from a microscopic scale. MD was developed by ALDER and WAINWRIGHT [19] in 1957 based on the phase transition for a hard sphere system. The energy and dynamics information are calculated in MD by solving the molecular motion equations [20,21]. Thus, the molecular motions of the oil−water interface can be simulated. The properties and removal mechanism of oil−water mixed system can be clarified from the molecular sight. ZHANG et al [22] used MD to study the distribution and diffusion behavior of microscopic particles at different oil−water interfaces. The effects of different particles and concentrations on the molecular diffusion behavior and oil−water interface morphology were obtained. GOODARZI et al [23,24] combined molecular dynamics and dissipative particle dynamics to simulate different types of oil−surfactant−water interface behaviors. It was found that the surface tension was the largest when the water−oil volume ratio was 1:1. The above studies have explored the characteristics of oil−water interface. However, the molecular motion of the oil−water mixed system at different temperatures is still unclear. The properties and morphological changes of the oil−surfactant−water system during the distillation process have not been explored.

In summary, there is currently no research on the removal of oil and water from aluminum chips through distillation. And the interface behavior and removal mechanism of oil and water molecules during the distillation process have not been yet clear. In this study, the process of removing oil and water through distillation was optimized, and the mechanism of removing oil and water from aluminum chips was elucidated. The optimal process achieved a 99.7% oil−water removal rate, which laid a foundation of pretreatment and upgrading regeneration of aluminum machining chips in industry. In this work, the properties of water and oil on chips were detected by thermo-gravimetric analysis (TGA) and energy dispersive spectroscopy (EDS). The parameters of distillation were optimized by response surface method (RSM). The system of oil−water was established with triethanolamine oleic acid soap, octane, and water molecules. And the mixture system was simulated by MD from room temperature to 377 °C to understand the molecular motion during distillation. Results show that the removal rate of water and oil is up to 99.7% when heating at 370 °C for 70 min with 3 cm loading thickness. And the mechanism of water and oil removal is a process of interface instability and separation.

## 2 Experimental

### 2.1 Materials and methods

The raw materials were 7050 aluminum alloy machining chips provided by Boeing, China. The morphology of chips is shown in Figs. 1(a, b). The chips are curly and have a pungent smell. Liquid can be observed at the contact position between the chips and bag. The pretreatment process of chips is shown in Fig. 1(c). Firstly, most of the free cutting fluid on the surface is removed by centrifugation. The oil and water content of the aluminum chips after centrifugation is 2.6 wt.%, and then the residual oil and water are removed and collected by distillation. The clean chips can be recycled as secondary aluminum alloy. The collected oil and water can be reused as cutting fluid in the machining process.

The removal rate of oil and water was detected in this work along with the effects of distillation time, temperature, and aluminum chip loading thickness. And the parameters of distillation were

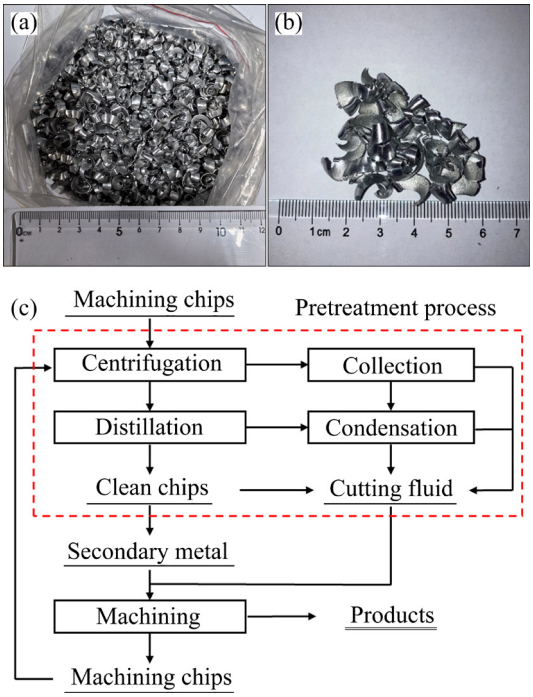


**Fig. 1** Morphology (a, b) and process flow (c) of recycling 7050 aluminum chips: (a) In bag; (b) Close-up; (c) Process flow

optimized by RSM. RSM is extensively used in the experimental optimization of resources regeneration, medical research, biological materials, chemical industry, metallurgical engineering, environmental science, and other disciplines [25−29]. It can reflect the cross-effects of various influencing factors in the system [30], avoid the isolation of manual experimental data, significantly reduce the experimental costs and improve efficiency. Design−Expert (Version 11.1.2.0) and Box−Behnken−Design (BBD) were applied in this work. The heating time, temperature and loading thickness of the aluminum chips were selected as three independent factors. The removal rate of oil and water was selected as the response value. Then, 17 sets of response experiments were designed according to BBD, and the optimal parameters were obtained by analyzing the fitting equation and the response surface.

## 2.2 Characterization

A vacuum tube furnace (GSL−1700X, KeJing, China) with continuous argon flow was used to measure the content of water and oil on the chips. The temperature was set to be 500 °C at 5 °C/min for fully remove the oil and water on the chips. The content of oil and water is calculated by Eq. (1):

$$\alpha=\frac{m_1-m_2}{m_2}\times 100\% \quad (1)$$

where $\alpha$ (%) is the oil and water content of aluminum chips; $m_1$ (g) and $m_2$ (g) are the mass of aluminum chips before and after roasting.

A box type resistance furnace (S90, KDF, Japan) was used to remove the oil and water from chips and detect the removal rate. The chips were weighed after each treatment to obtain the mass reduction $\Delta m$, and the removal rate can be calculated by Eq. (2):

$$r=\frac{\Delta m}{m_0\alpha}\times 100\% \quad (2)$$

where $r$ (%) is the removal rate of oil and water, $\Delta m$ (g) is the mass reduction of aluminum chips after distillation treatment, and $m_0$ (g) is the original mass of aluminum chips before distillation treatment.

The Soxhlet extraction method was used to extract the cutting oil on the surface of aluminum chips for 5 h in a 70 °C water bath. The Soxhlet extractor was manufactured by Beijing Chemical Glass Instrument Station, China. And the extractant was petroleum ether with a low-boiling point of 30−60 °C, purchased from Sinopharm Chemical Reagent Co., Ltd. After the extraction, the cutting oil was analyzed by the thermogravimetric instrument (TG209F3, Netzsch, Germany) in the Thermogravimetric Analysis Laboratory of the Beijing University of Science and Technology Analysis and Testing Center, China. Scanning electron microscope (SEM, MERLIN VP Compact, Carl Zeiss, Jena, Germany) and energy spectrum analysis (EDS) were used to analyze the deposits on the surface of aluminum chips.

## 2.3 Simulation methods

### 2.3.1 Molecular model and optimization

Materials Studio 2019 software was applied for MD simulations with Visualizer, Forcite and Amorphous Cell modules. COMPASS II was used as force field in this calculation. COMPASS was developed by SUN [31], which can well handle the solution system containing organic and inorganic molecules. The atom-based method was used to calculate electrostatic force and van der Waals force (vdW). The cutoff distance was set to be 15.5 Å.

Smart method was used as the algorithm. Triethanolamine oleic acid soap molecule, $C_{24}H_{47}NO_4$, was selected as the surfactant molecule, which was a kind of non-ionic surfactant commonly used as the emulsifier of metal cutting fluids. Octane, $C_8H_{18}$, was used as oil molecule coherent with predecessors [23,32], which was mainly used as industrial organic solvents. Materials Visualizer module was used to draw 3D models of triethanolamine oleic acid soap, octane, and water molecules. Then, the geometry optimization task in the Forcite module was used to optimize the molecular models to minimize the energy. After that, the intermolecular binding energy can be calculated by Eq. (3) [33]:

$$|E_{\text{inter}}|=|E_{\text{total}}-(E_1+E_2)| \quad (3)$$

where $E_{\text{inter}}$ represents the binding energy between molecules, $E_{\text{total}}$ represents the total energy of the two molecules, and $E_1$ and $E_2$ represent the energy when the molecules exist independently. The energy when the three molecules exist independently was obtained through the optimized molecular model. The geometry optimization task of the Forcite module was performed to calculate $E_{\text{total}}$.

2.3.2 Molecular dynamics simulation

Amorphous cell module was used to construct the oil−surfactant−water system for simulating the behavior of the real mixed solution system of cutting fluid. The optimized triethanolamine oleic acid soap molecules, octane molecules and water molecules were imported into a cell with a cubic boundary condition. And the molecular ratio of triethanolamine oleic acid soap to oil and to water was 20:111:1000, so that the volume ratio of oil and water was 1:1. The initial and target density of the system was set to 0.6 and 0.8 g/cm$^3$, respectively. Then, the geometry optimization and the anneal tasks in the Forcite module were used to optimize the constructed system. The number of anneal cycles was set to be 5, the initial temperature was set to be 27 °C (300 K), the intermediate cycle temperature was set to be 327 °C (600 K), and the temperature gradient was 50 °C. In actual situation, the oil and water molecules were distilled in an open container at a certain temperature without the change of the molecular number and pressure. Therefore, in this simulation, the NPT ensemble was selected with the Nose temperature control method and Berendsen pressure control method. After annealing, the dynamics task in the Forcite module was used for molecular dynamics simulation. The time step was 1 fs with a total of $5\times10^5$ steps. The image was output every 1000 steps. The temperature was set to be 27, 77, 127, 177, 227, 277, 327 and 377 °C respectively to understand the mechanism of oil and water removal in distillation process.

## 3 Results and discussion

### 3.1 Properties of cutting oil

TG−DTG curves of extracted cutting oil are shown Fig. 2, where $T$ is the temperature (°C), $w$ is the mass fraction (%), and d$w$/d$T$ is the mass loss rate (%/°C). Figure 2 indicates that the mass loss of cutting oil is obvious between 200 and 300 °C. And the mass loss rate reaches a peak at 250 °C. In consideration of efficiency, it is determined that the temperature of removal oil and water should be not lower than 300 °C.

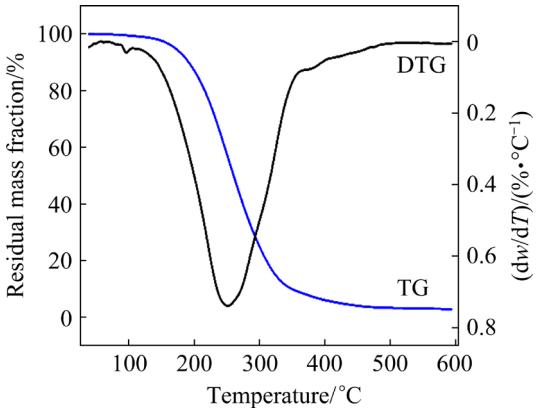


**Fig. 2** TG−DTG curves of cutting oil on surface of aluminum machining chips

However, there are lots of brown deposits on the surface of aluminum chips and at the bottom of the crucible when the temperature exceeds 400 °C, as shown in Figs. 3(a, b). Moreover, the color of these deposits becomes darker with the increase of temperature or time. The surface morphology and composition analysis results of these deposits are shown in Figs. 3(c, d). Figure 3(d) indicates that the element with the highest mass fraction in the deposits is carbon, followed by boron. The sources of borides are the salts added to the cutting oil, such as boron amine and sodium tetraborate. Those salts have high boiling points and cannot escape with the oil and water vapor so that they have no effect on removal rate. During the melting process of 7050 alloy, it is necessary to add Al−Ti−B to refine the

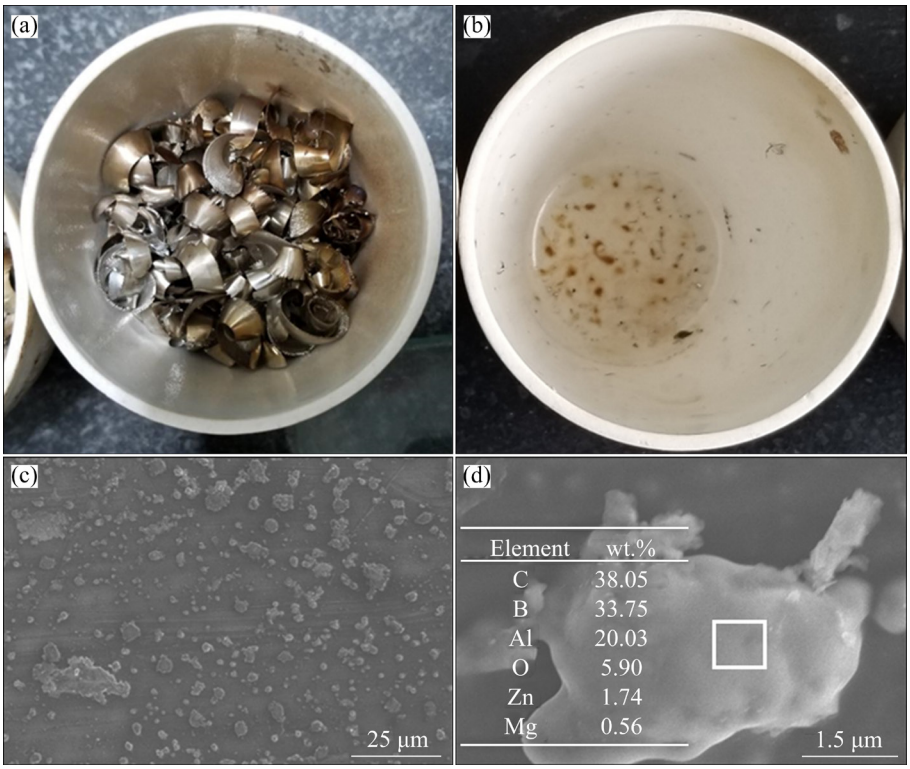


**Fig. 3** Morphologies of aluminum chips at 450 °C: (a) Chips; (b) Crucible; (c) SEM image of chips; (d) EDS data

grains [34,35]. Therefore, boron can play a role in refining grains in 7050 alloys. The carbon comes from the incompletely burned alkanes of the cutting oil. Therefore, it can be inferred that the cutting oil will be carbonized and deposited on the surface of chips when the distillation temperature exceeds 400 °C. These carbides reduce $\Delta m$ value in Eq. (2), resulting in a reduction of removal rate, and the chips are polluted by the carbides. Therefore, the temperature of distillation for aluminum chips should be controlled between 300 and 400 °C.

### 3.2 Optimization by response surface method

Aluminum machining chips are put into the vortex well of the double-chamber furnace as light and thin materials in recycled aluminum factories. The feeding speed of chips should be able to realize the submerged melting in the vortex well. Considering the efficiency of factory and the adaptability of continuous production equipment, 1−5 cm loading thickness and 20−80 min heating time were adopted as the variable range. According to the above test results, temperature ($A$), time ($B$), loading thickness ($C$) and coded level are shown in Table 1. The design of BBD and results are shown in Table 2, where $\eta$ represents the response value (removal rate). In order to reduce the unknown effects, the experimental design includes 12 sets of variable experiments and 5 repeated axial points. And the order of experiments is randomized.

**Table 1** Independent factors of BBD

| Factor | Independent variable | Coded level | | |
|---|---|---|---|---|
| | | −1 | 0 | 1 |
| $A$ | Temperature/°C | 300 | 350 | 400 |
| $B$ | Time/min | 20 | 50 | 80 |
| $C$ | Thickness/cm | 1 | 3 | 5 |

Then, the coded equation is fitted by quadratic model, as shown in Eq. (4), where $A$, $B$ and $C$ are the coded factors in Table 1. It can be seen from Eq. (4) that the coefficient of the linear factors $A$ and $B$ and the interaction of $BC$ are positive. The coefficients of the linear factor $C$ and the interaction of $AB$ and $AC$ are negative. It is included that the interaction of temperature and time, and the interaction of time and loading thickness can increase the removal rate. The loading thickness and the interaction of time and temperature have a negative impact on the removal rate. The fitted equation is consistent with the real situation.

**Table 2** Experiments and results of BBD

| Std. order | Run order | Factor 1, $A$/°C | Factor 2, $B$/min | Factor 3, $C$/cm | Response, $\eta$/% |
|---|---|---|---|---|---|
| 4 | 1 | 400 | 80 | 3 | 92.5 |
| 15 | 2 | 350 | 50 | 3 | 98.4 |
| 10 | 3 | 350 | 80 | 1 | 88.1 |
| 5 | 4 | 300 | 50 | 1 | 79.5 |
| 14 | 5 | 350 | 50 | 3 | 100.0 |
| 8 | 6 | 400 | 50 | 5 | 98.6 |
| 7 | 7 | 300 | 50 | 5 | 79.9 |
| 3 | 8 | 300 | 80 | 3 | 85.8 |
| 6 | 9 | 400 | 50 | 1 | 100.0 |
| 11 | 10 | 350 | 20 | 5 | 76.0 |
| 9 | 11 | 350 | 20 | 1 | 89.8 |
| 2 | 12 | 400 | 20 | 3 | 85.8 |
| 13 | 13 | 350 | 50 | 3 | 100.0 |
| 12 | 14 | 350 | 80 | 5 | 97.5 |
| 1 | 15 | 300 | 20 | 3 | 62.9 |
| 17 | 16 | 350 | 50 | 3 | 99.5 |
| 16 | 17 | 350 | 50 | 3 | 97.0 |

$$\eta_1=98.98+8.60A+6.18B-0.675C-4.05AB-0.45AC+5.80BC-7.79A^2-9.44B^2-1.69C^2 \quad (4)$$

Analysis of variance (ANOVA) was performed to judge the accuracy of the model. The results of ANOVA for this BBD design are shown in Table 3. The $F$-value of the model is 44.24, indicating that the model is significant. The $P$-value of the model is less than 0.0001. If the $P$-value is less than 0.0500, the model is meaningful and accurate. The lack of fit is not significant, meaning that the model is accurate with real data. $F$-value of the lack of fit is 5.04 and $P$-value is 0.0761, which imply that there is a 7.61% chance for a lack of fit $F$-value to occur due to noise. That may be due to the error of repeated central test, e.g., the Std. 16th result of 350 °C, 50 min and 3 cm test is 97%, which deviates from the results of other groups at the same parameters. The fitting coefficient ($R^2$) of this model is 0.9827, indicating that the accuracy of the quadratic model is credible in statistical analysis. With the same operation process, the model can meet 98.27% of the experimental data. The predicted $R^2$ of 0.7758 and the adjusted $R^2$ of 0.9605 are reasonable with a difference less than 0.2. The signal-to-noise ratio of this model is 22.2837, which is significantly greater than 4, meaning that the data are accurate in fitting. The coefficient of variation (C.V.) in this model is 2.36%, significantly lower than 15%, indicating that the operation of the experimental process is credible and the response value (removal rate) is stable. By further analyzing the $P$-values in the quadratic equation from the ANOVA results, it is found that items $A$, $B$, $BC$, $A^2$ and $B^2$ have significant effects

**Table 3** ANOVA results of fitted model in BBD

| Source | Sum of squares | Mean square | $F$-value | $P$-value | Significance |
|---|---|---|---|---|---|
| Model | 1796.19 | 199.58 | 44.24 | < 0.0001 | Significant |
| $A$ | 591.68 | 591.68 | 131.16 | < 0.0001 | |
| $B$ | 305.05 | 305.05 | 67.62 | < 0.0001 | |
| $C$ | 3.64 | 3.64 | 0.8080 | 0.3986 | |
| $AB$ | 65.61 | 65.61 | 14.54 | 0.0066 | |
| $AC$ | 0.8100 | 0.8100 | 0.1796 | 0.6845 | |
| $BC$ | 134.56 | 134.56 | 29.83 | 0.0009 | |
| $A^2$ | 255.51 | 255.51 | 56.64 | 0.0001 | |
| $B^2$ | 375.22 | 375.22 | 83.18 | < 0.0001 | |
| $C^2$ | 12.03 | 12.03 | 2.67 | 0.1465 | |
| Residual | 31.58 | 4.51 | | | |
| Lack of fit | 24.97 | 8.32 | 5.04 | 0.0761 | Not significant |
| Pure error | 6.61 | 1.65 | | | |

on the removal rate. In summary, the equation is accurate in fitting. The model and the fitted equation can be used to analyze and optimize the influence of three independent factors on the removal rate.

Design Expert was used to perform three-dimensional surface analysis, and the results are shown in Fig. 4. With the help of three-dimensional surface model analysis, the impact of interactions between the three factors on the removal rate can be more intuitively and clearly expressed.

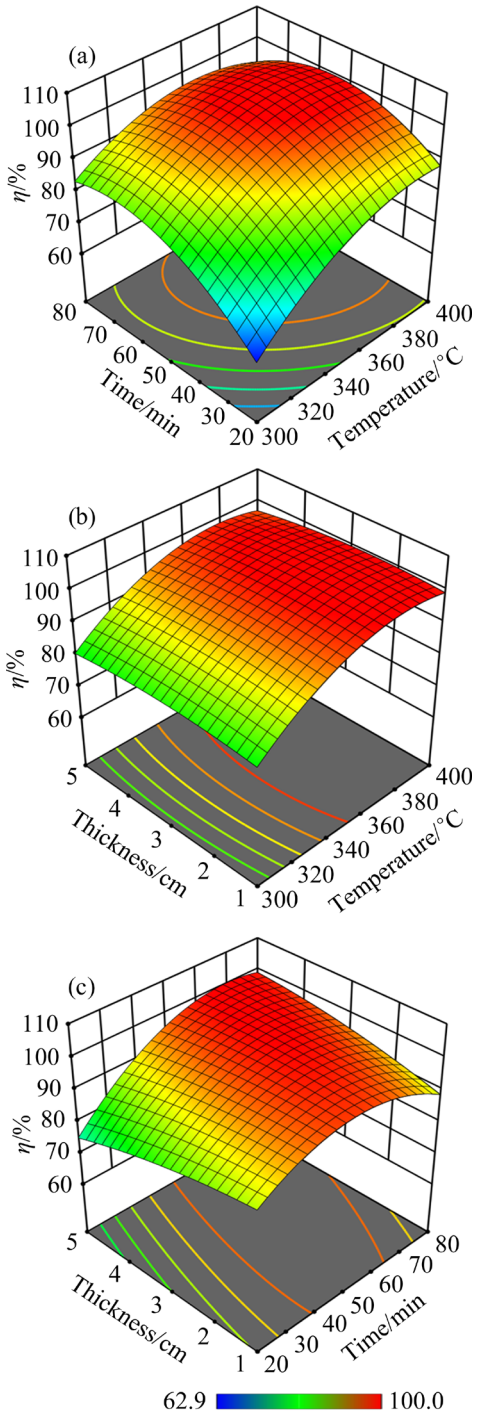


**Fig. 4** Three-dimensional response surface results: (a) Influence of time and temperature on removal rate ($C$=3 cm); (b) Influence of temperature and loading thickness on removal rate ($B$=50 min); (c) Influence of time and loading thickness on removal rate ($A$=350 °C)

The effect of time and temperature on the removal rate is shown in Fig. 4(a). The surface is steep with a large curvature, indicating that the temperature and time have a significant influence on the removal rate. With the increase of temperature and time, the removal rate gets higher; while the increasing speed becomes slower and stops at a specific point. Then, the removal rate shows a downward trend. It means that the cutting oil is carbonized and deposited on the surface of aluminum chips at a high temperature and/or a long heating time, which is consistent with the results discussed above. Figure 4(b) presents the influence of temperature and loading thickness on the removal rate. It can be clearly seen that the curved surface is inclined, meaning that the influence of temperature is greater than loading thickness. And the curved surface is flat with a small curvature, indicating that the interaction of loading thickness and temperature is weak. As the loading thickness of the aluminum chips increases, the removal rate shows a whole downward trend. The diffusion resistance of oil and water vapor becomes greater with the increase of thickness, which affects the removal rate in dynamics. On the other hand, with increasing temperature, the removal rate rises and then shows a downward trend. This trend is consistent with the previous analysis result that the increase of temperature will cause carbonization and deposition of alkanes, thus decreasing the removal rate. Figure 4(c) shows the influence of time and loading thickness. The curved surface is curly with a diagonal protrusion. It is inferred that the interaction between loading thickness and time is complicated. In a short heating time, the increase in the thickness of the aluminum chip will lead to the decrease of the removal rate. But when the heating time is longer, the increase in the loading thickness will slightly decrease the removal rate. Based on the previous analysis, long heating time can lead to the deposition and carbonization of the oil. With the increase of loading thickness, it is more difficult for oil and water to escape, resulting in more carbides on the surface of aluminum chips, thus causing the decrease of removal rate.

The optimized parameters of oil and water removal were determined by RSM combined with

the actual experimental conditions of 370 °C, 70 min, and 3 cm loading thickness. Three sets of verification experiments were carried out in parallel under optimized conditions. The average removal rate is 99.7%. The surfaces of aluminum chips and crucibles are clean with no pollution, as shown in Supplementary Materials (SM) in Fig. S1.

### 3.3 Simulation results and removal mechanism

The binding energy between/among water, oil and surfactant molecules was calculated by molecular mechanics. The optimized molecular models are shown in Fig. S2(a) in SM. The relative molecular energy of triethanolamine oleic acid soap and octane molecules are $-7.63\times10^4$ and $-8.33\times10^4$ J/mol based on water molecule when they exist independently. The combination of molecules results in a decrease in energy. And the binding energy can represent the stability of the combination. The binding energies of different molecular interactions are shown in Table 4, where S represents triethanolamine oleic acid soap molecule, O represents the octane molecule, W represents the water molecule, and $E_{inter}$ represents the binding energy between the molecules. $E_{inter}$ is calculated according to Eq. (3), expressed as absolute values. It can be seen from Table 4 that the binding energies of S−O and S−W are far greater than that of W−O, respectively $3.30\times10^4$, $3.95\times10^4$ and $4.02\times10^3$ J/mol. The binding energy proves that the surfactant molecule has hydrophilicity and lipophilicity. The binding energy of octane molecules and water molecules is less than $4.18\times10^3$ J/mol. The water and oil molecules are not easy to combine so that there will be a stratification when water and oil coexist. The binding energy of triethanolamine oleic acid soap, octane and water molecules mixed model is $6.59\times10^4$ J/mol. It indicates that surfactants can reduce the total energy between oil and water, and stabilize the oil−water interface.

**Table 4** Binding energy between/among oil, water, and surfactant molecules

| System | $\lvert E_{inter}\rvert$/(J·mol$^{-1}$) |
|---|---|
| S−O | $3.30\times10^4$ |
| S−W | $3.95\times10^4$ |
| W−O | $4.02\times10^3$ |
| S−O−W | $6.59\times10^4$ |

The molecular dynamics simulation of the oil−water−surfactant mixed system was carried out according to the methods in Section 2.3. The results of MD provide a microscopic perspective to understand the mechanism of oil and water removal. The state of initial model is shown in Fig. S2(b) in SM, and the models after molecular dynamics simulation at different temperatures are shown in Figs. S2(c–j) in SM. A cubic (60 Å × 60 Å × 60 Å) was put in the interface of oil and water to clearly show the relative motions of oil, surfactant, and water, as shown in Figs. S2(b−j). The relative contents along the interface direction at 27, 77, 127, 177, 227 and 277 °C are shown in Fig. 5, where W represents water molecules, O represents oil molecules, SH represents the head (hydrophilic group) of surfactant molecules, and ST represents the carbon tail (lipophilic group) of surfactant molecules.

It can be seen from Figs. S2(c−f) and Fig. 5 that below 177 °C, water and oil molecules gather together respectively, forming a layered structure. As the temperature increases, some water molecules first evaporate and escape from the box, and then the layered structure of oil and water molecules is destroyed. At temperatures above 227 °C, the layered structure is significantly damaged, and a large number of water and oil molecules are dispersed. All types of molecules no longer aggregate but escape from the box, volatilizing into gas. A detailed insight into the oil−water interface is shown in Fig. 5. When the oil−water interface is stable, as shown in Figs. 5(a–d), the main peaks of ST relative content are located at the oil layer while the main peaks of SH are located at the water layer. The relative content further proves that the surfactant has hydrophilicity and lipophilicity: the carbon chains of triethanolamine oleic acid soap molecules insert into the octane layer while the hydroxyl groups of triethanolamine oleic acid soap contact with the water layer. So, surfactants can reduce the total energy between oil and water, stabilize the oil−water interface, which is in line with the discussion on Table 4. But the molecules are randomly distributed above 227 °C. The oil−water layer is obviously destroyed with the increase of temperature. The radial distribution function (RDF, $g(r)$) was analyzed at room temperature to further investigate the damage of oil−water stratification. The RDF describes the probability

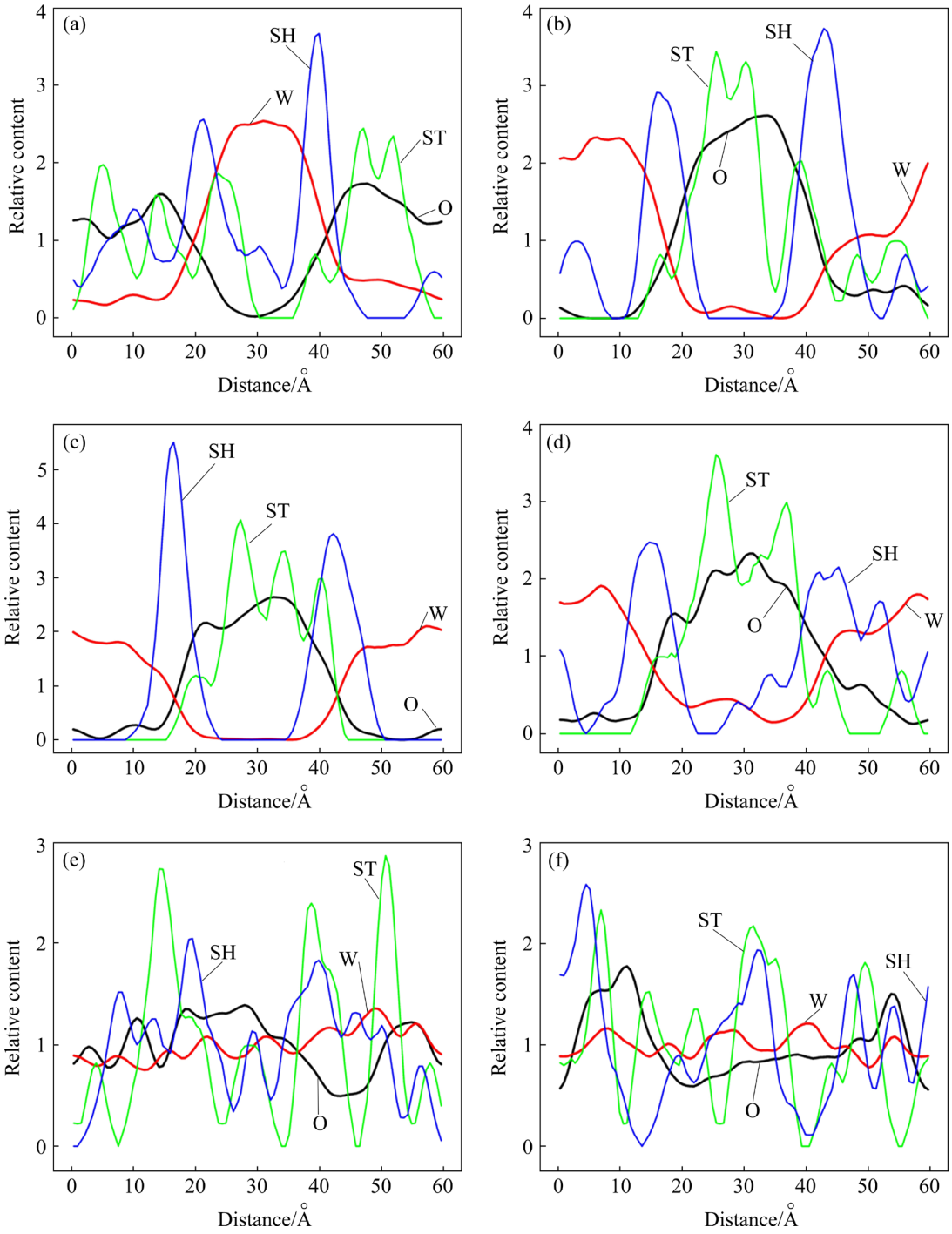


**Fig. 5** Relative contents of water (W), oil (O), hydrophilic group (SH) and lipophilic group (ST) of surfactant: (a) 27 °C; (b) 77 °C; (c) 127 °C; (d) 177 °C; (e) 227 °C; (f) 277 °C

density ($g_{A-B}(r)$) for finding A and B particles at a distance of $r$ when averaged over the sampling trajectory, as shown in Eq. (5) [36]:

$$g_{A-B}(r)=\left(\frac{n_B}{4\pi r^2 dr}\right)\Big/\left(\frac{N_B}{V}\right) \quad (5)$$

where $n_B$ is the number of B particles located at a distance $r$ from particle A in a shell of thickness d$r$, $N_B$ is the number of B particles in the system, and $V$ is the total volume of the system. The RDFs of H atoms in surfactant (represented by $H_S$) and O atoms in water (represented by $O_W$) and the O and H atoms in water (represented by $O_W$ and $H_W$) are shown in Fig. 6. There are peaks at 0.97, 1.77 and 3.25 Å in the $g(r)$ of H and O atom in water. The first peak is the bond length of H—O in water

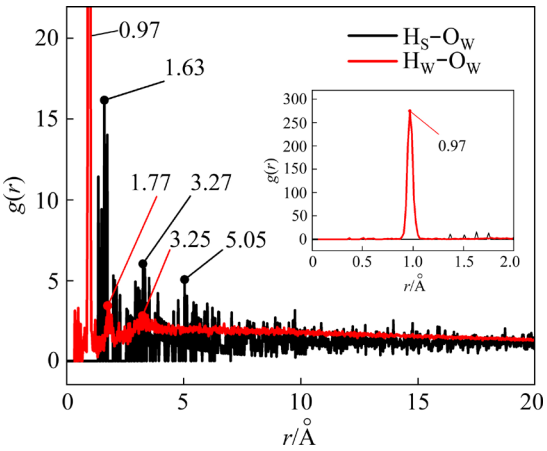


**Fig. 6** Radial distribution function results $g(r)$ of H atoms in surfactant ($H_S$) and O and H atoms in water ($O_W$ and $H_W$)

molecules. 3.25 Å is the length of O—H without hydrogen bond of water, and 1.77 Å is the bond length of O—H with hydrogen bond of water, which is consistent with the value of 1.78 Å in the simulation of LI et al [37]. There are peaks at 1.63, 3.27 and 5.05 Å in the $g(r)$ of $H_S$ and $O_W$ atoms. The first peak means that strong hydrogen bonding exists between $H_S$ and $O_W$ atoms. And the followed peaks show that there are strong and weak vdW between $H_S$ and $O_W$ atoms [38].

The mean squared displacement (MSD) and self-diffusion coefficient ($D$) were calculated to investigate the motion of molecules and the results are shown in Fig. 7. In MD, the proportionality constant that is related the MSD to the observation time is called the self-diffusivity, as shown in Eq. (6) [39].

$$D_i=\frac{1}{2d}\lim_{t\to\infty}\frac{<(x(t)-x(0))^2>_i}{t} \tag{6}$$

where $D_i$ is the self-diffusion coefficient of species $i$, $t$ is the time, $x$ is the position, and $d$ is the dimensionality of the system (for three-dimension simulation, $d$=3). The numerator of Eq. (6) is MSD. The angled brackets indicate that an ensemble average has been taken. The MSDs are all proportional to time and consistent with the Einstein equation [37]. Result shows that the MSD and $D$ of water are far greater than those of octane

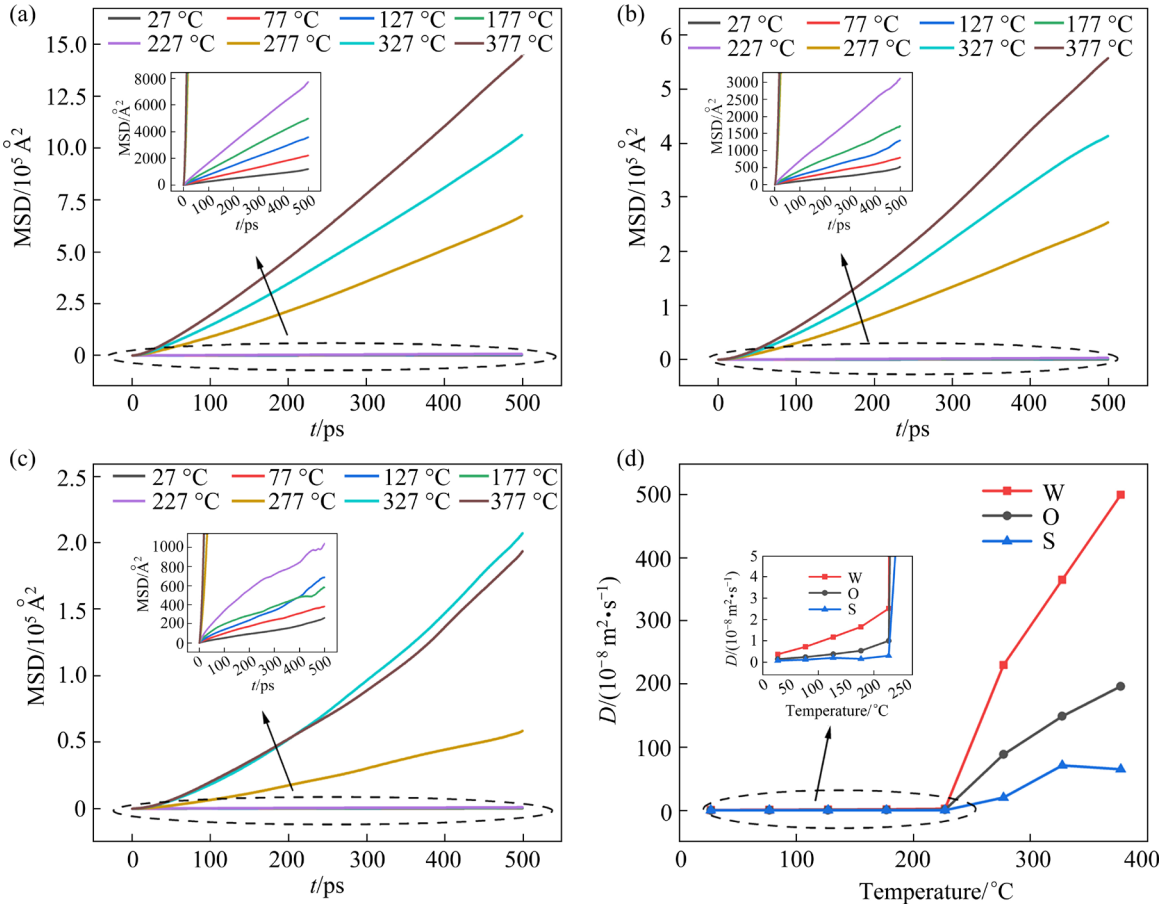


**Fig. 7** Mean squared displacement (MSD) of water (a), octane (b) and triethanolamine oleic acid soap (c) and self-diffusion coefficient (d)

and triethanolamine oleic acid soap. There is a sudden change of MSDs and diffusion coefficient at 227−277 °C. It can be inferred that the system has been transformed into gas at 227−277 °C so that the diffusion distance and diffusion ability are increased significantly. The results of MSD and *D* are consistent with the results of TGA and Fig. 5.

The analysis of density and energy versus temperature was carried out to systematically understand molecular behavior. The results are shown in Fig. 8. The density decreases with the increase of temperature as shown in Fig. 8(a). At 177 °C, the density of the whole system is lower than the octane density of 0.703 g/cm$^3$, indicating that some molecules have evaporated into gas at this time. At 227−277 °C, the density of the system decreases rapidly, indicating that most of the molecules have changed into gas, which is consistent with the TGA results. In Fig. 8(b), the kinetic energy increases linearly with the increase of temperature. The potential energy and total energy increase with the increase of temperature. But vdW energy decreases when the temperature increases. And there is a sharp increase of the potential energy and total energy but a large decrease of vdW energy at 227−277 °C. The vdW force is a "soft" Lennard−Jones 9-6 (L−J) potential [40] for intermolecular interaction in MD. The increase of molecular kinetic energy results in a larger molecular distance, so that L−J potential is weak and vdW energy gradually decreases. So, we can deduce that the weak interaction force is broken firstly with the increase of temperature, e.g., the vdW between $H_S$ and $O_W$ at 5.05 Å. While with higher temperature, strong interaction force begins to disintegrate, such as the strong hydrogen bonding between $H_S$ and $O_W$ at 1.63 Å, and the molecular distance further increases. Hydrogen bond is treated as part of the vdW force in the COMPASS force field [40]. Therefore, with the increase of temperature, the hydrogen bonds between/among $H_S$ and $O_W$ and water molecules are cut off, resulting in the sudden decrease of vdW energy at 227−277 °C. The sudden decrease of vdW energy is consistent with the previous discussion of RDF. We can conclude that the increase of temperature results in the decrease of vdW force and the increase of kinetic energy and molecular distance. Thus, the water−oil interface becomes unstable. Above 277 °C, hydrogen bonds and vdW force are mostly broken. The triethanolamine oleic acid soap, octane and water molecules are vaporized, which destroys the interface of oil and water and results in the separation of oil and water from the surface of aluminum machining chips. Therefore, the oil−water mixture can be completely removed from the solid surface by distillation. The mechanism of water and oil removal is a process of interface instability and separation.

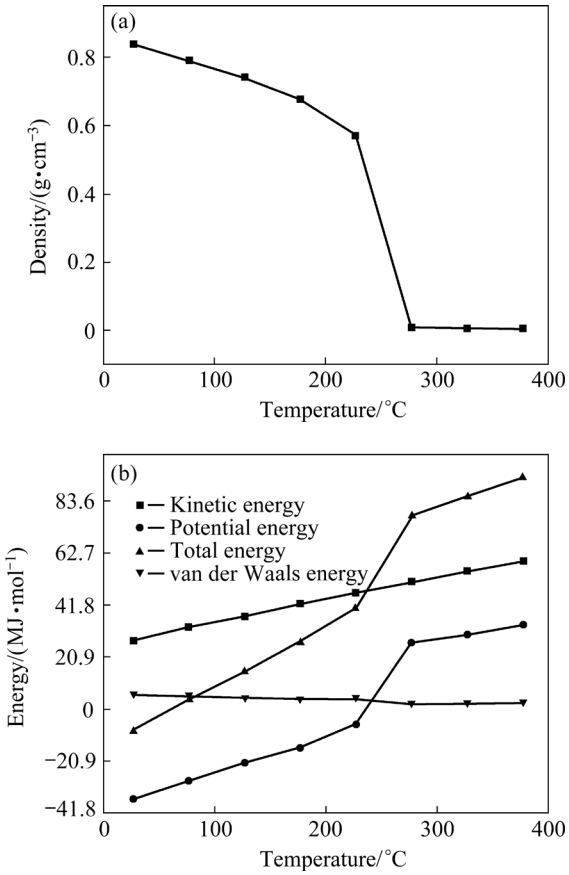


**Fig. 8** Results of density (a) and energy (b) versus temperature of molecular dynamics simulation for distillation process

## 4 Conclusions

(1) The cutting fluid is vaporized at 200−300 °C and carbonized over 400 °C. The removal rate of water and oil is up to 99.7% with no pollution when the chips are heated at 370 °C for 70 min at 3 cm loading thickness.

(2) A layered arrangement of water−surfactant−oil is formed at room temperature. There are strong hydrogen bonds, strong and weak vdW forces between O—H in triethanolamine oleic acid soap ($H_S$) and O atoms in water ($O_W$) at 1.63, 3.27 and 5.05 Å, respectively.

(3) The weak interaction vdW force is vanished and the strong hydrogen bonds are weakened with the increase of temperature. Hydrogen bonds and vdW force are broken above 277 °C, resulting in the destruction of layer arranged water−surfactant−oil system. The mechanism of water and oil removal is a process of interface instability and separation.

(4) The mechanism and processes of removing water and oil removal from aluminum chips were clarified through the combination of experiment and simulation. In the next step, the process of distillation can be optimized in industrial application for upgrading regeneration of aluminum machining chips.

## Acknowledgments

This work was sponsored by the National Key Research and Development Projects of China (Nos. 2021YFC1910504, 2019YFC1907101, 2019YFC1907103, 2017YFB0702304), the Key Research and Development Project in Ningxia Hui Autonomous Region, China (Nos. 2020BCE01001, 2021BEG01003), the Key and Normal Projects of National Natural Science Foundation of China (Nos. U2002212, 51672024), Xijiang Innovation and Entrepreneurship Team, China (No. 2017A0109004), and the Fundamental Research Funds for the Central Universities, China (Nos. FRF-BD-20-24A, FRF-TP-20-031A1, FRF-IC-19-017Z, FRF-GF-19-032B, 06500141).

## Supplementary Materials

Supplementary materials in this paper can be found at: http://tnmsc.csu.edu.cn/download/22-p3871-2023-0189-Supplementary_Materials.pdf.

## References

[1] PUGA H, BARBOSA J, SOARES D, SILVA F, RIBEIRO S. Recycling of aluminium swarf by direct incorporation in aluminium melts [J]. Journal of Materials Processing Technology, 2009, 209(11): 5195−5203.

[2] SHAMSUDIN S, LAJIS M, ZHONG Z W. Evolutionary in solid state recycling techniques of aluminium: A review [J]. Procedia CIRP, 2016, 40: 256−261.

[3] CHIBA R, YOSHIMURA M. Solid-state recycling of aluminium alloy swarf into c-channel by hot extrusion [J]. Journal of Manufacturing Processes, 2015, 17: 1−8.

[4] CHIBA R, NAKAMURA T, KURODA M. Solid-state recycling of aluminium alloy swarf through cold profile extrusion and cold rolling [J]. Journal of Materials Processing Technology, 2011, 211(11): 1878−1887.

[5] BEHNAGH R A, FATHI F, YEGANEH M, PAYDAR M, MOHAMMAD M A, LIAO Y L. Production of seamless tube from aluminum machining chips via double-step friction stir consolidation [J]. The International Journal of Advanced Manufacturing Technology, 2019, 104: 4769−4777.

[6] GÜLEY V, KHALIFA N B, TEKKAYA A E. Direct recycling of 1050 aluminum alloy scrap material mixed with 6060 aluminum alloy chips by hot extrusion [J]. International Journal of Material Forming, 2010, 3(1): 853−856.

[7] HONG Jing-min, ISMAIL Z Z, HONG Jing-lan. Environmental and economic assessment of recycled aluminum alloy production—A case study of China [J]. Advanced Materials Research, 2010, 146/147: 1027−1030.

[8] MOUNGOMO J B M, NGANGA-KOUYA D, SONGMENE V, KOUAM J, KENNÉ J P. Machinability study of recycled aluminum cans and machining chips [J]. The International Journal of Advanced Manufacturing Technology, 2016, 87: 2551−2566.

[9] SILVA L R, CORRÊA E C S, BRANDÃO J R, ÁVILA R F. Environmentally friendly manufacturing: Behavior analysis of minimum quantity of lubricant MQL in grinding process [J]. Journal of Cleaner Production, 2020, 256: 103287.

[10] ZHU Y X, CHAPPUIS L B, KLEINE R D, KIM H C, WALLINGTON T J, LUCKEY G, COOPER D R. The coming wave of aluminum sheet scrap from vehicle recycling in the United States [J]. Resources, Conservation and Recycling, 2021, 164: 105208.

[11] LI Xiao-jiang, WANG Li, LU Hong-sheng, WANG Na, WANG Bao-gang, HUANG Zhi-yu. Using a switchable water to improve sustainable extraction for oil sands by low-concentration surfactant solution [J]. Journal of Cleaner Production, 2021, 292: 126045.

[12] GUPTA N K. Biodiesel production from waste cooking oil ssing mechanical stirring and ultrasonic cavitation method [J]. IOP Conference Series: Materials Science and Engineering, 2021, 1116: 012067.

[13] KHAMIS S S, LAJIS M A, ALBERT R A O. A sustainable direct recycling of aluminum chip (AA6061) in hot press forging employing response surface methodology [J]. Procedia CIRP, 2015, 26: 477−481.

[14] PANDEY A K, PRAJAPATI N, NAYAK K C, DATE P P. Sustainable manufacturing process for recycling of aluminum alloy waste into direct product by high-pressure torsion process [J]. Materials Today: Proceedings, 2019, 18: 3099−3108.

[15] HYODO A, BOLFARINI C, ISHIKAWA T T. Chemistry and tensile properties of a recycled AA7050 via spray forming and ECAP/E [J]. Materials Research, 2012, 15(5): 739−748.

[16] KORE A S, NAYAK K C, DATE P P. Formability of aluminium sheets manufactured by solid state recycling [J]. Journal of Physics: Conference Series, 2017, 896: 012007.

[17] SIMON L, MORAES C A M, MODOLO R C E, VARGAS M, CALHEIRO D, BREHM F A. Recycling of contaminated metallic chip based on eco-efficiency and eco-effectiveness approaches [J]. Journal of Cleaner Production, 2017, 153: 417−424.

[18] LEE C M, CHOI Y H, HA J H, WOO W S. Eco-friendly technology for recycling of cutting fluids and metal chips: A review [J]. International Journal of Precision Engineering and Manufacturing, 2017, 4(4): 457−468.

[19] ALDER B J, WAINWRIGHT T E. Phase transition for a hard sphere system [J]. The Journal of Chemical Physics, 1957, 27(5): 1208−1209.

[20] HE Y J, MA Bin. Molecular dynamics analysis on bending mechanical behavior of alumina nanowires at different loading rates [J]. Transactions of Nonferrous Metals Society of China, 2022, 32(11): 3687−3698.

[21] JIANG Bin, DONG Zhi-hua, ZHANG Ang, SONG Jiang-feng, PAN Fu-sheng. Recent advances in micro-alloyed wrought magnesium alloys: Theory and design [J]. Transactions of Nonferrous Metals Society of China, 2022, 32(6): 1741−1780.

[22] ZHANG Cheng-bin, DAI Han-hui, LU Peng-fei, WU Liang-yu, ZHOU Bo, YU Cheng. Molecular dynamics simulation of distribution and diffusion behaviour of oil−water interfaces [J]. Molecules, 2019, 24(10): 1905.

[23] GOODARZI F, KONDORI J, REZAEI N, ZENDEHBOUDI S. Meso- and molecular-scale modeling to provide new insights into interfacial and structural properties of hydrocarbon/water/surfactant systems [J]. Journal of Molecular Liquids, 2019, 295: 111357.

[24] GOODARZI F, ZENDEHBOUDI S. Effects of salt and surfactant on interfacial characteristics of water/oil systems: Molecular dynamic simulations and dissipative particle dynamics [J]. Industrial and Engineering Chemistry Research, 2019, 58: 8817−8834.

[25] LELA B, KROLO J, JOZIĆ S. Mathematical modeling of solid-state recycling of aluminum chips [J]. The International Journal of Advanced Manufacturing Technology, 2016, 87: 1125−1133.

[26] WITTENHAGEN L, MATTINGLEY J B. Steady-state visual evoked potentials reveal enhanced neural responses to illusory surfaces during a concurrent visual attention task [J]. Cortex, 2019, 117: 217−227.

[27] BELHAJ D, FRIKHA D, ATHMOUNI K, JERBI B, AHMED M B, BOUALLAGUI Z, KALLEL M, MAALEJ S, ZHOU J, AYADI H. Box−Behnken design for extraction optimization of crude polysaccharides from Tunisian Phormidium versicolor cyanobacteria (NCC 466): Partial characterization, in vitro antioxidant and antimicrobial activities [J]. International Journal of Biological Macromolecules, 2017, 105: 1501−1510.

[28] DANDEKAR A, ROBERTS Z A, PAULSON S, CHEN W N, SON S F, KOSLOWSKI M. The effect of the particle surface and binder properties on the response of polymer bonded explosives at low impact velocities [J]. Computational Materials Science, 2019, 166: 170−178.

[29] CHAKRABORTY V, DAS P, ROY P K. Carbonaceous materials synthesized from thermally treated waste materials and its application for the treatment of strontium metal solution: Batch and optimization using response surface methodology [J]. Environmental Technology & Innovation, 2019, 15: 100394.

[30] LU Yan, SONG Qing-ming, XU Zhen-ming. Integrated technology for recovering Au from waste memory module by chlorination process: Selective leaching, extraction, and distillation [J]. Journal of Cleaner Production, 2017, 161: 30−39.

[31] SUN H. An ab initio force-field optimized for condensed-phase applications—Overview with details on alkane and benzene compounds [J]. Journal of Physical Chemistry B, 1998, 102(38): 7338−7364.

[32] WANG Shu-yan, YANG Shan-wen, WANG Rui-chen, TIAN Rui-chao, ZHANG Xiao-yu, SUN Qi-ji, LIU Li-li. Dissipative particle dynamics study on the temperature dependent interfacial tension in surfactant−oil−water mixtures [J]. Journal of Petroleum Science and Engineering, 2018, 169: 81−95.

[33] AHN D H, PARK C, SONG J W. Predicting whether aromatic molecules would prefer to enter a carbon nanotube: A density functional theory study [J]. Journal of Computational Chemistry, 2020, 41(13): 1261−1270.

[34] XIAO Hong-yu, LI Yu-gang, GENG Ji-wei, LI Hong-ping, WANG Ming-liang, CHEN Dong, LI Zhu-guo, WANG Hao-wei. Effects of nano-sized $TiB_2$ particles and $Al_3Zr$ dispersoids on microstructure and mechanical properties of Al−Zn−Mg−Cu based materials [J]. Transactions of Nonferrous Metals Society of China, 2021, 31(8): 2189−2207.

[35] GHADIMI H, NEDJHAD S H, EGHBALI B. Enhanced grain refinement of cast aluminum alloy by thermal and mechanical treatment of Al−5Ti−B master alloy [J]. Transactions of Nonferrous Metals Society of China, 2013, 23(6): 1563−1569.

[36] CHENG Dong-cai, HUANG Zhi-xiong, YE Zhang-ji, REN Run-tao, WANG Jing-jing, HUANG Chong-su. Study of the equilibrium swelling of poly(methyl methacrylate-co-*n*-butyl methacrylate) immersed in water via MD simulation [J]. Chemical Engineering Science, 2017, 173: 483−492.

[37] LI Di, LIU Feng-hai, JIA Guo-zhu. Energy transformation and dynamic properties of N, N-dimethylformamide aqueous solution under E/M field using NNVE MD simulations [J]. Fluid Phase Equilibria, 2018, 474: 76−82.

[38] WANG Na, HUANG Xin, GONG Hao, ZHOU Ya-nan, LI Xin, LI Fei, BAO Ying, XIE Chuang, WANG Zhao, YIN Qiu-xiang, HAO Hong-xun. Thermodynamic mechanism of selective cocrystallization explored by MD simulation and phase diagram analysis [J]. AIChE Journal, 2019, 65(5): 16570.

[39] GHAFFARI A, KELISHAMI A R. MD simulation and evaluation of the self-diffusion coefficients in aqueous NaCl solutions at different temperatures and concentrations [J]. Journal of Molecular Liquids, 2013, 187: 238−245.

[40] BUNTE S W, SUN H. Molecular modeling of energetic materials: The parameterization and validation of nitrate esters in the COMPASS force field [J]. Journal of Physical Chemistry B, 2000, 104(11): 2477−2489.

# 分子动力学模拟和实验研究铝屑脱油、水技术及机理

王建文[1]，张深根[1]，刘 波[1,2]，沈汉林[1]，陈 宁[3]，邬博宇[1]，刘 君[1,4]，阎昭辉[5]

1. 北京科技大学 新材料技术研究院，北京 100083；
2. 新疆有色金属研究所，乌鲁木齐 830009；
3. 北京科技大学 材料科学与工程学院，北京 100083；
4. 肇庆市大正铝业有限公司，肇庆 526200；
5. 山东南山铝业股份有限公司，龙口 265713

**摘 要：**通过热重分析、扫描电子显微镜、响应曲面和分子动力学等方法，阐明铝屑脱油脱水的过程和机理。结果表明，铝屑表面切削液在 200～300 ℃质量损失明显，超过 400 ℃时被碳化。水、表面活性剂和油分子在室温下分层排列。表面活性剂中的 O—H 和水中的 O 原子之间分别在 1.63、3.27 和 5.05 Å 处存在强氢键、强范德华力和弱范德华力。随着温度的升高，弱范德华力相互作用消失，氢键减弱。超过 277 ℃时强范德华力和氢键被破坏，导致水−表面活性剂−油分层界面的失稳及破坏。在 370 ℃和 3 cm 装料厚度下加热 70 min 时，铝屑的油、水脱除率达 99.7%。

**关键词：**脱水；脱油；机加工屑；分子界面；再生铝合金；机理

**(Edited by Wei-ping CHEN)**